Available online at www.sciencedirect.com

SciVerse ScienceDirect

Procedia IUTAM 5 (2012) 99 – 107

Procedia IUTAM

www.elsevier.com/locate/procedia

IUTAM Symposium on 50 Years of Chaos: Applied and Theoretical

Augmented Lorenz Equations as Physical Model for Chaotic Gas Turbine

T. Miyano, K. Cho, Y. Okada, J. Tatsutani, T. Toriyama

Depaertment of Mechanical Engineering, Ritsumeikan University, 1-1-1 Noji-Higashi, Kusatsu, Shiga 525-8577, Japan

Abstract

Motivated by the chaotic waterwheel subject to the Lorenz equations, which was invented by Malkus and Howard about 40 years ago, we have developed a chaotic gas turbine by mechanically simulating the Rayleigh-Bénard convection of fluids heated from below and cooled from above. The rotational motion of the turbine erratically reverses its direction similarly to the random reversal of large-scale circulation in turbulent thermal convection at high Rayleigh numbers. The nondimensionalized expression for the equations of motion of our gas turbine is represented as a starlike network of many Lorenz subsystems sharing the dimensionless angular velocity of the turbine rotor as the central node, referred to as augmented Lorenz equations. We report the observed motion of the turbine and discuss its dynamical properties.

Keywords: Lorenz equations; turbulence; gas turbine; chaotic waterwheel; large-scale circulation

1. Introduction

The Lorenz model is a simplified dynamical model of the Rayleigh-Bénard (RB) convection of a fluid heated from below and cooled from above [1]. Assuming the convective flow to be a two-dimensional roll, the Lorenz model consists of nondimensionalized ordinary differential equations that determine the time evolutions of three independent dimensionless variables X, Y and Z, where X represents the velocity field and Y and Z represent characteristics of the thermal field. The model is derived from the Boussinesq equations [2] and retains some of the physical aspects of RB convection by incorporating the reduced Rayleigh number, the Prandtl number and the geometric parameter (as a function of the aspect ratio). Despite its simplicity, the Lorenz model is an epoch-making breakthrough in nonlinear science that has

1877-7058 © 2012 Published by Elsevier Ltd. Selection and/or Peer-review under responsibility of Takashi Hikihara and Tsutomu Kambe
doi:10.1016/j.piutam.2012.06.013

provided a firm platform on which many important studies on chaos and its applications have been performed.

About 40 years ago, Malkus and Howard invented a chaotic waterwheel whose rotational motion exactly follows the Lorenz equations with a geometric parameter of unity, corresponding to an aspect ratio of $\sqrt{3}$ in RB convection [3, 4]. The chaotic waterwheel randomly reverses its direction of rotation, which is a mechanical realization of the chaotic behavior of X in the Lorenz model. Motivated by the chaotic waterwheel, we have recently developed a chaotic gas turbine that erratically reverses its direction of rotation similarly to the chaotic waterwheel [5, 6]. Our gas turbine simulates the mechanism of RB convection in that buoyancy, viscous drag and thermal dissipation are mechanically simulated by the aerodynamic drag generated on the turbine blades by an air flow, the frictional force generated on the turbine rotor by a thrust bearing and the leakage of the air flow out of the turbine, respectively. As will be shown in this paper, unlike the chaotic waterwheel, the equations of motion of our gas turbine turn out to be an infinite-dimensional system of ordinary differential equations whose nondimensionalized expression is represented by a starlike network of infinitely many Lorenz subsystems sharing the dimensionless angular velocity of the rotor as the central node. The nondimensionalized equations with the number of Lorenz subsystems truncated at N are referred to as augmented Lorenz equations. The temporal fluctuation of the angular velocity of the rotor is reminiscent of the random reversal of large-scale circulation, often called mean wind, in turbulent RB convection at a high Rayleigh number exceeding 10^6 with an aspect ratio on the order of unity [7–24].

In this paper, we report experimental results for the chaotic motion of our gas turbine operated under various conditions and compare the experimental results with the corresponding numerical solutions of our equations of motion. The bifurcation structure of the turbine motion is analyzed on the basis of the augmented Lorenz equations. This paper is organized as follows. A brief description of the mechanical structure of our machine and the equations of motion together with their nondimensionalized expression are given in section 2. Details will be given in [6]. Section 3 presents experimental results of the angular velocity as a function of time and the corresponding numerical solutions generated by numerically integrating the equations of motion given in section 2. The bifurcation structure of the system is also presented. Sections 4 and 5 provide a discussion and conclusions, respectively.

2. Chaotic Gas Turbine and Its Equations of Motion

Figures 1 (a) and (b) show a photograph of our gas turbine and a schematic drawing of its mechanical structure, respectively. The turbine includes a stainless steel disc rotor with a diameter of 40 [mm]. The rotor is sandwiched by three acrylic plates. There are 24 thin blades on the rotor arranged with radial symmetry. This arrangement of the turbine blades generates aerodynamic drag but no aerodynamic lift, to allow the buoyancy in RB convection to be simulated, unlike existing planar-type micro gas turbines [25, 26]. Air is provided through the top inlet and exhausted through the bottom outlet. The air inflow impinges on the turbine blades near the inlet within an angle of $\pm\phi$ [rad] from the central horizontal axis of the turbine. Part of the air leaks out through the narrow channels between the upper acrylic plate and the rotor, which simulates the thermal dissipation in RB convection. A hydrostatic thrust bearing is used to generate a frictional force between the rotor and the acrylic plates to simulate the viscous drag in RB convection. This bearing includes a circular array of six register holes through which pressurized air is fed to the bearing gap to push up the rotor to above the lower acrylic plate. As the hydrostatic thrust pressure increases, the frictional force decreases.

We next give the equations of motion of the turbine rotor. Details of the derivation of the equations will be given elsewhere [6]. Here, a summary is given.

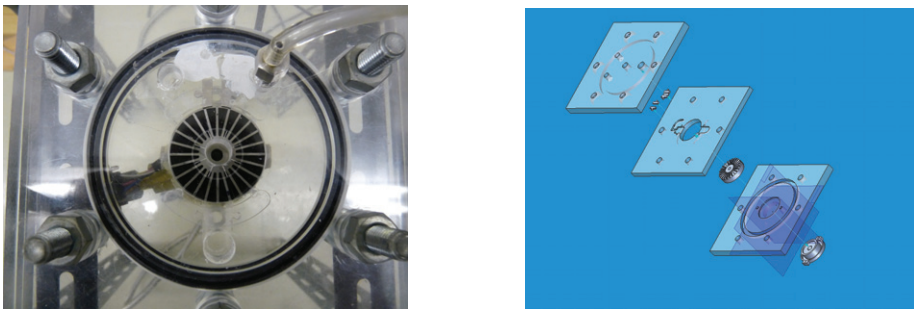

(a) (b)

Fig. 1. (a) Photograph of chaotic gas turbine. (b) Schematic of chaotic gas turbine.

$$\dot{a}_n = n\omega b_n - (K+\alpha)a_n, \tag{1}$$

$$\dot{b}_n = -n\omega a_n - (K+\alpha)b_n + \frac{2\alpha P_{in}}{n\pi}\sin n\phi, \tag{2}$$

$$I\dot{\omega} = -v\omega + Sra_1\left(\phi - \frac{1}{2}\sin 2\phi\right) + \sum_{n=2}^{N}\left[\frac{1}{n-1}a_n Sr\{sin(n-1)\phi\} - \frac{1}{n+1}a_n Sr\{\sin(n+1)\phi\}\right], \tag{3}$$

where $a_n(t)$ and $b_n(t)$ respectively denote the nth time-dependent sinusoidal and cosinusoidal coefficients of the spatial Fourier expansion of the air inflow pressure around the central axis of the turbine, $\omega(t)$ [rad/sec] is the angular velocity of the rotor, α [1/sec] is the rate of air inflow near the turbine blades, K [1/sec] is the rate of air leakage, P_{in} [Pa] is the air inflow pressure (gauge pressure), I [kgm^2] is the inertial moment of the rotor estimated assuming a negligible mass for each turbine blade, v [kgm^2/sec] is the damping constant of the hydrostatic bearing, S [m^2] is the area of each turbine blade and r[m] is the effective radius of the rotor to which the torque due to aerodynamic drag is applied. The Fourier expansion is truncated at N to conduct numerical simulations. The parameter settings fixed in the numerical simulations are summarized in Table 1. For the parameters v, r, K and α, we have no experimental method for estimating their exact values at present. The values of the parameters given in Table 1 were estimated. However, these parameter settings reproduce the observed angular velocity as a function of time, as shown in the next section.

Table 1. Parameter settings.

Parameter	Setting	Physical unit
S	2.0×10^{-5}	m^2
r	0.015	m
ϕ	0.36	rad
I	1.5×10^{-5}	kgm^2
K	0.01	sec^{-1}
α	0.03	sec^{-1}

We introduce the following dimensionless variables:

$$\mathbf{a}=\begin{pmatrix} a_1 & \cdots & 0 \\ \vdots & \ddots & \vdots \\ 0 & \cdots & a_N \end{pmatrix},\ \mathbf{b}=\begin{pmatrix} b_1 & \cdots & 0 \\ \vdots & \ddots & \vdots \\ 0 & \cdots & b_N \end{pmatrix},\ \mathbf{n}=\begin{pmatrix} 1 & \cdots & 0 \\ \vdots & \ddots & \vdots \\ 0 & \cdots & N \end{pmatrix},\ \mathbf{W}=\begin{pmatrix} \sin\phi & \cdots & 0 \\ \vdots & \ddots & \vdots \\ 0 & \cdots & \sin N\phi \end{pmatrix},$$

$$\mathbf{\Phi}=\begin{pmatrix} \phi-\frac{1}{2}\sin 2\phi & \cdots & 0 \\ \vdots & \ddots & \vdots \\ 0 & \cdots & \frac{1}{N}\sin(N-1)\,\phi-\frac{1}{N+1}\sin(N+1)\phi \end{pmatrix},$$

$$\mathbf{a}=\mathbf{\delta Y}\,,$$

$$\mathbf{b}=\mathbf{\beta Z}+\frac{2\alpha P_{in}}{(K+\alpha)\pi}\mathbf{n^{-1}W}\,,$$

$$\omega=tr(\mathbf{\gamma X}),$$

$$t=T\tau\,,$$

$$X=\ tr(\mathbf{n^{-1}n^{-1}X})\,.$$

Straightforward calculations lead to a nondimensionalized expression for the equations of motion as

$$\frac{dX}{d\tau}=\sigma\{tr(\mathbf{n^{-1}n^{-1}Y})-X\}\,, \tag{4}$$

$$\frac{d\mathbf{Y}}{d\tau}=\mathbf{R}X-\mathbf{nZ}X-\mathbf{Y}\,, \tag{5}$$

$$\frac{d\mathbf{Z}}{d\tau}=\mathbf{nY}X-\mathbf{Z}\,, \tag{6}$$

where the scalar variable X is the dimensionless angular velocity of the rotor, the diagonal components of $N\times N$ diagonal matrices $\mathbf{Y}$ and $\mathbf{Z}$ are the dimensionless sinusoidal and cosinusoidal Fourier coefficients corresponding $a_n(t)$ and $b_n(t)$, respectively,

$$\mathbf{Y}=\begin{pmatrix} Y_1 & \cdots & 0 \\ \vdots & \ddots & \vdots \\ 0 & \cdots & Y_N \end{pmatrix},$$

$$\mathbf{Z}=\begin{pmatrix} Z_1 & \cdots & 0 \\ \vdots & \ddots & \vdots \\ 0 & \cdots & Z_N \end{pmatrix},$$

and σ and R_0 are constants defined by

$$\sigma=\frac{v}{I(K+\alpha)}\,, \tag{7}$$

$$\mathbf{R}=R_0\mathbf{n}^2\mathbf{\Phi W}\,, \tag{8}$$

$$R_0=\frac{2\alpha SrP_{in}}{(K+\alpha)^2v\pi}\,. \tag{9}$$

Equations (4) – (6) are exactly equivalent to the Lorenz equations with a geometric parameter of unity when the Fourier expansion is truncated at $N=1$. Hence, the coefficients σ and R_0 defined using the mechanical parameters of the turbine correspond to the Prandtl number and the reduced Rayleigh number, respectively. Thus, Eqs. (4) – (6) are referred to as augmented Lorenz equations. Note that the augmented Lorenz equations can be viewed as a starlike network of N Lorenz subsystems sharing X as the central node. Extended versions of the Lorenz model were previously studied by McLaughlin and Martin [27] and Curry [28]. Curry extended the Lorenz model by simplifying the Boussinesq equations using a 14-

mode truncation. McLaughlin and Martin developed an extended model consisting of more coupled variables than those in Curry's model to examine the transition to turbulence. These previous models are different from our model.

3. Results

We operated the turbine under various air inflow pressures and thrust pressures and recorded videos of the operating turbine rotor. The angular velocity of the rotor was estimated as a time series with a sampling time interval of 33 [msec] using image processing to record the trajectory of a mark on the rotor. Figure 2 (a) shows a time series of the angular velocity actually observed under an air inflow pressure of 20 [kPa], a thrust pressure of 2.5 [kPa] and $N = 100$. Random reversal of the direction of rotational motion can be seen. We numerically integrated Eqs. (1) – (3) using the 4th-order Runge-Kutta method with a time width of 1 [msec]. The initial values of a_n and b_n are given as Gaussian random numbers with mean 0 and variance 1, and $\omega(0) = 0$. To eliminate the initial transient part, the first 200,000 data points were discarded. Figure 2 (b) shows numerical solutions under $P_{\mathrm{in}} = 20\ [\mathrm{kPa}]$, $v = 1.5 \times 10^{-5}\ [\mathrm{kgm^2/sec}]$ and $N = 100$, corresponding to Fig.2 (a). The numerical solutions capture the general features of the corresponding observed time series. Figure 3 shows observed and numerical results for the maximum magnitude of angular velocity as a function of air inflow pressure (P_{in}). In our experiments, an initial small tilt of the rotor caused a finite difference in the friction between the rotor and the acrylic plates despite the same thrust pressure being applied. This induced substantially different settings of v in each operation of the turbine. For this reason, there are differences between the observed results and numerical solutions in Fig. 3.

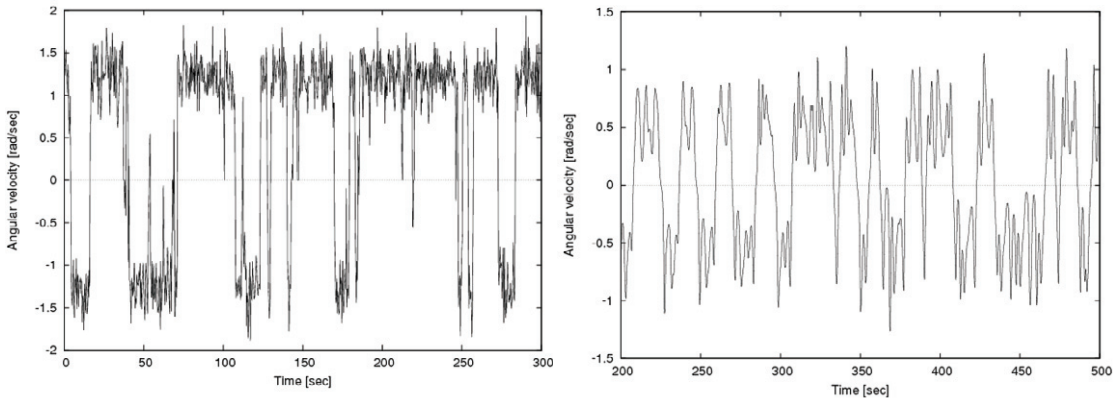

(a) (b)

Fig. 2. (a) Observed angular velocity as function of time (air inflow pressure = 20 [kPa], thrust pressure = 2.5 [kPa]). (b) Numerical estimates of angular velocity as function of time ($P_{\mathrm{in}} = 20$ [kPa]], $v = 1.5 \times 10^{-5}$ [kgm^2/sec], N = 100).

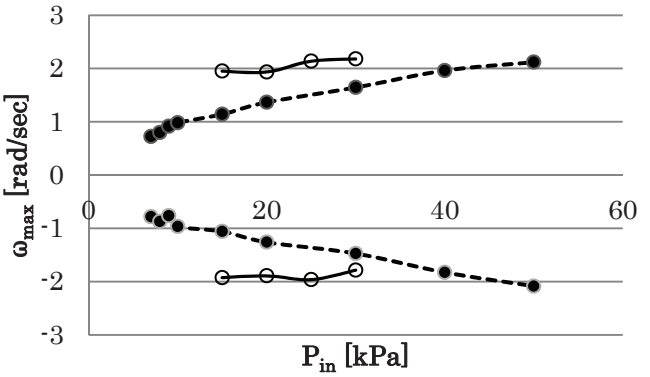

Fig. 3. Maximum magnitude of angular velocity as function of air inflow pressure. Experimental observations at a thrust pressure of 2.5 [kPa] are indicated by solid lines and open circles. Numerical estimates with $\nu = 1.5 \times 10^{-5}$ [kgm^2/sec] and $N = 100$ are indicated by dashed lines and closed circles.

Nevertheless, the general tendency is reproduced by our equations of motion. Figure 4 (a) shows the observed maximum magnitude of angular velocity as a function of thrust pressure under an air inflow pressure of 20 [kPa]. The corresponding numerical results calculated with $P_{\mathrm{in}} = 20$ [kPa] and $N = 100$ are shown in Fig.4 (b). An exact comparison between the results in Figs.4 (a) and (b) cannot be performed because of the lack of a method for estimating ν from the applied thrust pressure. Nevertheless, the general features of Fig.4 (a) appear to be reproduced in Fig.4 (b).

To examine how the combination of the Prandtl number σ and the reduced Rayleigh number R_0 determines the chaotic region of turbine motion, we applied the augmented Lorenz equations (4) – (6) with various R_0 and σ at a dimensionless time width of 4×10^{-5}. To reduce the computational time, N was set to $N = 10$.By examining the dynamical behaviour of the solutions of X, we identified the boundary pairs of R_0 and σ that divide the chaotic region of X from the nonchaotic region. Results are shown in Fig.5 as solid lines and + symbols.

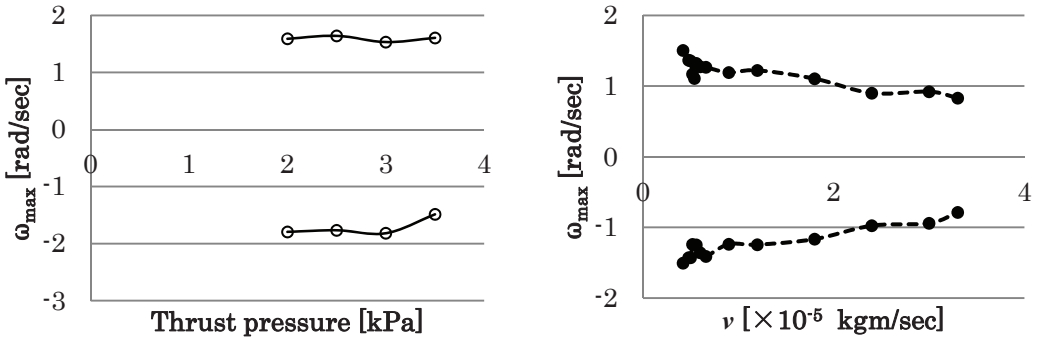

(a) (b)

Fig. 4. (a) Observed maximum magnitude of angular velocity as function of thrust pressure (air inflow pressure = 20 [kPa]).
(b) Numerical estimates of maximum magnitude of angular velocity as function of damping rate of hydrostatic bearing ($P_{\mathrm{in}} = 20$ [kPa], $N = 100$).

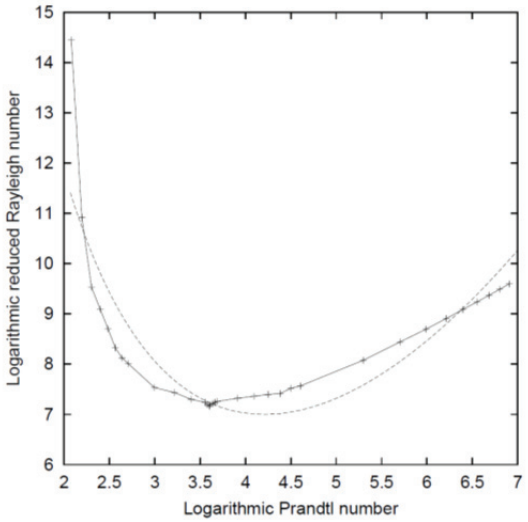

Fig. 5. Boundary curve delineating chaotic region of turbine motion: $\log R_0$ as function of $\log \sigma$. The chaotic region is above the solid curve passing through the + symbols. The fitting curve is indicated by a dashed line.

To obtain an analytical expression for the boundary curve, the plots in Fig.5 were fitted by the approximating function

$$\log R_0 = \frac{a}{\log \sigma} + b(\log \sigma)^2 + c\,, \tag{10}$$

where a, b and c are constants. These constants were estimated to be $a = 28.37$, $b = 0.19$, $c = -3.11$ using the least-mean-squares method. The fitting curve is also shown in Fig.5 as a dashed line.

4. Discussion

Although our machine is based on the chaotic waterwheel, the equations of motion governing our machine are considerably different from those of the chaotic waterwheel. This difference stems from the restriction of the working range of aerodynamic drag on the turbine blades to within $\pm\phi$ [rad] from the central horizontal axis of the turbine. In the chaotic waterwheel, there is no such restriction on the gravitational force of the water working as the driving force to rotate the waterwheel. The restriction of the working range results in nonvanishing contributions of all Fourier coefficients $a(\mathrm{t})$ and $b(\mathrm{t})$ in our turbine, which leads to the characteristic structure of the augmented Lorenz equations.

The dynamical property of the turbine motion, i.e., that of the dimensionless angular velocity X depends on ϕ. Once ϕ is fixed, however, the dynamical property of X is entirely determined by two parameters, σ and R_0. These dimensionless parameters correspond to the Prandtl number and the reduced Rayleigh number, respectively, because the augmented Lorenz model is equivalent to the Lorenz model when $N = 1$, i.e., when the Fourier coefficients Y_{n} and Z_{n} are truncated at the first order. In this sense, the augmented Lorenz model inherits the dynamical nature of the Lorenz model. For instance, our recent study has verified that a pair of augmented Lorenz oscillators with direct coupling via X or $\mathbf{Y}$ can synchronize with each other. The augmented Lorenz model is a nondimensionalized model and can hence be used as a general dynamical model in other applications such as chaos-based secure communications.

Our equations of motion reproduce the main features of the motion of the turbine, which was designed to mechanically simulate the RB convection. Hence, the augmented Lorenz model is considered to capture some aspects of RB convection. In fact, the angular velocity as a function of time shown in Figs.2

(a) and (b) is reminiscent of the temporal fluctuation of the velocity field previously observed by Sreenivasan et al. for the large-scale circulation of cryogenic helium gas with a high Rayleigh number of $\sim 10^{11}$ and an aspect ratio of unity [13]. Our recent study has shown some similarities between the statistical properties of our results for the angular velocity of the rotor and previous observations of the velocity field, which suggests the possibility of using the augmented Lorenz model as a dynamical model for the random reversal of large-scale circulation through cessation in turbulent RB convection [6]. Thus, we may be able to estimate the Reynolds number *Re* for the rotational motion of the rotor using the empirical relationship among *Re*, the Prandtl number *Pr* and the Rayleigh number *Ra* reported by Niemela and Sreenivasan [14]:

$$Re = f(\Gamma) Pr^{-0.7} Ra^{0.49}, \tag{11}$$

where $f(\Gamma) \approx 0.2$ when the aspect ratio Γ of RB convection is on the order of unity. The geometric parameter of unity specifying the augmented Lorenz model corresponds to $\Gamma = \sqrt{3}$. Hence, $f(\Gamma) = 0.2$, $Pr = \sigma$ and $Ra = R_0 \times 1708$ upon the assumption of solid boundary conditions in our model.

5. Conclusion

We have developed a chaotic gas turbine subject to augmented Lorenz equations that have a starlike network of many Lorenz subsystems. Our model can reproduce the main features of the random reversal of the turbine rotor, which is reminiscent of that of large-scale circulation in turbulent RB convection at high Rayleigh numbers. The mathematical relationship between the augmented Lorenz model and the Boussinesq equations is an open question. Applications of the augmented Lorenz model also remain to be investigated in future studies.

Acknowledgements

We thank Dr. Hiroshi Gotoda for stimulating discussion and helpful advice. This study was supported by JSPS Grant-in-Aid for Scientific Research No.22500214.

References

[1] Lorenz EN, Deterministic nonperiodic flow. *J Atmos Sci* 1963; **20**: 130–141.

[2] Saltzman B, Finite amplitude free convection as an initial value problem -I. *J Atmos Sci* 1962; **19**: 329–341.

[3] Kolár M, Gumbs G, Theory for the experimental observation of chaos in a rotating waterwheel. *Phys Rev* A 1992; **45**: 626–637.

[4] Strogatz SH, *Nonlinear Dynamics and Chaos.* Perseus Books Publishing; 1994.

[5] A video of our chaotic gas turbine under operation can be seen at the following URL: http://www.ritsumei.ac.jp/se/~tmiyano/index_english.html.

[6] Cho K, Miyano T, Toriyama T, Chaotic gas turbine subject to augmented Lorenz equations, submitted.

[7] Kadanoff LP, Turbulent heat flow: structures and scaling. *Physics Today* August 2001: 34–39.

[8] Ahlers G, Grossmann S, Lohse D, Heat transfer and large scale dynamics in turbulent Rayleigh-Bénard convection. *Rev Mod Phys* 2009; **81**: 503–537.

[9] Niemela JJ, Skrbek L, Sreenivasan KR, Donnelly RJ, Turbulent convection at very high Rayleigh numbers. *Nature* 2000; **404**: 837–840.

[10] Chavanne X, Chillá F, Chabaud B, Castaing B, Hébral B, Turbulent Rayleigh-Bénard convection in gaseous and liquid He. *Phys Fluids* 2001; **13**: 1300–1320.

[11] Zhang J, Childress S, Libchaber A, Non-Boussinesq effect: Thermal convection with broken symmetry. *Phys Fluids* 2001; **9**: 1034–1042.

[12] Niemela JJ, Skrbek L, Sreevivasan KR, Donnelly RJ, The wind in confined thermal convection. *J Fluid Mech* 2001; **449**: 169–178.

[13] Sreenivasan KR, Bershadskii A, Niemela JJ, Mean wind and its reversal in thermal convection. *Phys Rev* E 2002; **65**: 056306.

[14] Niemela JJ, Sreenivasan KR, Confined turbulent convection. *J Fluid Mech* 2003; **481**: 355–384.

[15] Tsuji Y, Mizuno T, Mashiko T, Sano M, Mean wind in convective turbulence of mercury. *Phys Rev Lett* 2005; **94**: 034501.

[16] Benzi R, Flow reversal in a simple dynamical model of turbulence. *Phys Rev Lett* 2005; 95: 024502.

[17] Fontenele Araujo F, Grossmann S, Lohse D, Wind reversals in turbulent Rayleigh-Bénard convection. *Phys Rev Lett* 2005; **95**: 084502.

[18] Brown E, Nikolaenko A, Ahlers G, Reorientation of the large-scale circulation in turbulent Rayleigh-Bénard convection. *Phys Rev Lett* 2005; **95**: 084503.

[19] Resagk C, du Puits R, Thess A, Dolzhansky FV, Grossmann S, Fontenele Araujo F, Lohse D, Oscillations of the large scale wind in turbulent thermal convection. *Phys Fluids* 2006; **18**: 095105.

[20] Brown E, Ahlers G, Large-scale circulation model for turbulent Rayleigh-Bénard convection. *Phys Rev Lett* 2007; **989**: 134501.

[21] Brown E, Ahlers G, A model of diffusion in a potential well for the dynamics of the large-scale circulation in turbulent Rayleigh-Bénard convection. *Phys Fluids* 2008; **20**: 075101.

[22] Brown E, Ahlers G, Azimuthal asymmetries of the large-scale circulation in turbulent Rayleigh-Bénard convection. *Phys Fluids* 2008; **20**: 105105.

[23] He X, Tong P, Measurements of the thermal dissipation field in turbulent Rayleigh-Bénard convection. *Phys Rev* E 2009; **79**: 026306.

[24] Bershadskii A, Chaos from turbulence: Stochastic-chaotic equilibrium in turbulent convection at high Rayleigh numbers. *Chaos* 2010; **20**: 043124.

[25] Epstein AH, Senturia SD, Macro power from micro machinery. *Science* 1997; **276**: 1211.

[26] Epstein AH, Millimeter-Scale, Micro-electro-mechanical systems gas turbine engines. *J Eng Gas Turbines Power* 2004; **226**: 205–226.

[27] McLaughlin JB and Martin PC, Transition to turbulence in a statistically stressed fluid system. *Phys Rev* A 1975; **12**: 186–203.

[28] Curry JH, A Generalized Lorenz system. *Commun Math Phys* 1978; **60**: 193–204.